Hydrological behavior of a deep sub-vertical fault in crystalline basement and relationships with surrounding reservoirs

Clément Roques, Olivier Bour, Luc Aquilina, Benoît Dewandel, Sarah Leray, Jean Michel Schroetter, Laurent Longuevergne, Tanguy Le Borgne, Rebecca Hochreutener, Thierry Labasque, et al.

1

1 HYDROLOGICAL BEHAVIOR OF A DEEP SUB-VERTICAL FAULT IN
2 CRYSTALLINE BASEMENT AND RELATIONSHIPS WITH
3 SURROUNDING RESERVOIRS

4 C. ROQUES*(1), O. BOUR(1), L. AQUILINA(1), B. DEWANDEL(2), S. LERAY(1), JM.

5 SCHROETTER(3), L. LONGUEVERGNE(1), T. LE BORGNE(1), R. HOCHREUTENER(1), T.

6 LABASQUE(1), N. LAVENANT(1), V. VERGNAUD-AYRAUD(1), B. MOUGIN(3)

7 *(1) Université Rennes 1-CNRS, OSUR-Géosciences Rennes, avenue du Général Leclerc, 35000 Rennes,*

8 *France*

9 *(2) BRGM, Water Dept., New Water Resource & Economy Unit, 1039, Rue de Pinville, 34 000*

10 *Montpellier, France*

11 *(3) BRGM, French Regional Geological Survey of French Brittany, Rennes Atalante Beaulieu 2 rue de*

12 *Jouanet, 35700 Rennes, France*

13 ** Corresponding author: Clément Roques, Université Rennes 1 – CNRS, OSUR Géosciences Rennes, 263*

14 *avenue du Général Leclerc, 35000 Rennes, France.*

15 *Email: clement.roques@univ-rennes1.fr*

16 *Phone: (0033)2.23.23.54.69.*

17 *Fax: (0033)2.23.23.60.90.*

18

19   ABSTRACT

20   Crystalline-rock aquifers generally yield limited groundwater resources. However, some highly

21   productive aquifers may be encountered, typically near tectonic discontinuities. In this study, we

22   used a multidisciplinary experimental field approach to investigate the hydrogeological behavior of a

23   sub-vertical permeable fault zone identified by lineament mapping. We particularly focused our

24   investigations on the hydrogeological interactions with neighboring reservoirs.

25   The geometry of the permeable domains was identified from geological information and hydraulic

26   test interpretations. The system was characterized under natural conditions and during a 9-week

27   large-scale pumping test. We used a combination of piezometric analysis, flow logs, groundwater

28   dating and tracer tests to describe the interactions between permeable domains and the general

29   hydrodynamical behaviors.

30   A clear vertical compartmentalization and a strong spatial heterogeneity of permeability are

31   highlighted. Under ambient conditions, the vertical permeable fault zone allows discharge of deep

32   groundwater flows within the superficial permeable domain. The estimated flow across the total

33   length of the fault zone ranged from 170 to 200 m^3/day. Under pumping conditions, hydrological

34   data and groundwater dating clearly indicated a flow inversion. The fault zone appears to be highly

35   dependent on the surrounding reservoirs which mainly ensure its recharge. Groundwater fluxes were

36   estimated from tracer tests interpretation. This study demonstrates the hydrogeological capacities of

37   a sub-vertical fault aquifer in a crystalline context. By describing the hydrological behavior of a fault

38   zone, this study provides important constrain about groundwater management and protection of

39   such resources.

40   **Keywords:** Hydrogeology, crystalline rocks, lineament, fault zone, large scale pumping test,

41   sustainable groundwater resource.

42

1 INTRODUCTION

Crystalline rocks cover large areas throughout the world of about 35% of the continental surface (Amiotte Suchet et al., 2003; Blatt and Jones, 1975) and may constitute a crucial water resource for vast population. The porosity and permeability of primary crystalline rocks are extremely low, but their hydraulic properties can be greatly modified as a result of secondary physical processes (unloading, tectonic activities…) and/or geochemical processes such as weathering, fluid circulation (Bahat, 1999; Caine et al., 1996; Evans et al., 1997; Henriksen and Braathen, 2005; Taylor and Howard, 2002, 1999)… Various conceptual models of hydrogeological compartmentalization in crystalline rock aquifers have been proposed (Chilton and Foster, 1995; Dewandel et al., 2006; Maréchal and Wyns, 2004; Taylor and Howard, 1999; Wyns et al., 2004). They usually consist of two main reservoirs: 1) a layer of alterites (<15 meters bgs), identified as a specific reservoir with a relatively high porosity and storage, highly sensitive to rainfall recharge; 2) a superficial fractured zone, of various thickness and which may be characterized by relatively dense sub-horizontal and sub-vertical fracturing. This fractured reservoir has in general a higher permeability although well yields are typically limited to less than 10 m^3/h.

However, highly productive zones have been locally highlighted in regions exposed to past or current tectonic activity, such as Brittany. In practice, although controversial (Gleeson and Novakowski, 2009), hydrogeologists often use fracture outcropping analysis or "lineaments" mapping to determine drilling localization, especially when such lineaments result from extensive tectonic activity (Gleeson and Novakowski, 2009; Henriksen and Braathen, 2005; Sander, 2006; Singhal and Gupta, 2010). Many factors must be considered to ensure the viability of the resource such as rock lithology affected by tectonic activity, stress fields and intensity of deformation. Such factors and fluid flow processes determine fault zone permeability (Caine et al., 1996; Evans et al., 1997; Gleeson and Novakowski, 2009; Goddard and Evans, 1995). Few hydrogeological studies examined relationships between lineaments structures, hydrogeological flow organization and productivity

68   wells (Fernandes and Rudolph, 2001; Henriksen and Braathen, 2005; Holland and Witthüser, 2011;

69   Richard et al., 2002; Sander, 2006). Fault zones may act as conduits, barriers, or as combined

70   conduit-barrier systems that enhance or impede fluid flow (Bense and Person, 2006; Caine et al.,

71   1996) but can also significantly influence groundwater flow, spring discharge, and water-table

72   elevations (Apaydin, 2010; Gleeson and Novakowski, 2009; Melchiorre et al., 1999).

73   In some cases, aquifers near highly conductive fault zones and with relatively high production rates

74   for crystalline rocks (from 20 to 100 m^3/h) have been described: Ploemeur aquifer, Brittany (Le

75   Borgne et al., 2006a; Leray et al., 2013; Ruelleu et al., 2010), the New Hampshire Bedrock Aquifer

76   (Richard et al., 2002), Crystalline Rock Aquifers in New England (Harte et al., 2008) and in the

77   Limpopo Province of South Africa (Holland and Witthüser, 2011).

78   The hydrodynamic functioning of fault structures in various geological contexts has been investigated

79   in several studies. In sedimentary media, Bense et al. (2006; 2003) showed the important effects of

80   the geometry and anisotropy of a fault zone on its hydraulic properties. Numerical studies, such as

81   those by Anderson et al. (Anderson and Bakker, 2008), also highlighted the influence of a vertical

82   fault on groundwater flow. In the crystalline context, some studies have described the permeability

83   architecture and hydrogeological functioning of fault zones for groundwater resources (Boutt et al.,

84   2010; Caine and Tomusiak, 2003; Evans et al., 1997; Ganerod et al., 2008; Stober and Bucher, 1999)

85   or hydrocarbon entrapment (Aydin, 2000). However, very few studies have analyzed the hydrological

86   functioning of faults in a water abstraction context. In this context, aquifer yields will mainly depend

87   on the ability of interactions between the fault and the surrounding reservoirs to allow recharge and

88   water availability. On the other hand, groundwater abstraction from a deep resource will

89   undoubtedly modify the hydrodynamic gradients and lead to mixing between the different

90   reservoirs. The hydrogeological influence of deep fault zones on overlaying reservoirs is poorly

91   known and is apparently difficult to characterize by field studies (Banwart et al., 1994; Carucci et al.,

92   2012; Folch and Mas-Pla, 2008; Gannon et al., 2011; Sophocleous, 2002). This question has been

93   tackled out only through few numerical studies, which have reported the hydrological efficiency of

94   fault zones to act as preferential flow zone that enhances recharge processes from surrounding

95   reservoirs (Folch and Mas-Pla, 2008; Leray et al., 2013).

96   The first aim of this study is to characterize the hydrodynamic functioning of a sub-vertical

97   permeable fault zone in crystalline basement from a large-scale field experiment. The main

98   objectives are to i)describe the architecture of the aquifer system, ii) define the flow organization

99   between the permeable zones and recharge processes towards the deep fault zone under natural

100   and pumping conditions and iii) characterize the origin of groundwater and mixing processes due to

101   groundwater abstraction. The experiment is carried out on a specific field site in Brittany (Western

102   France), identified by lineament observation (Carn-Dheilly and Thomas, 2008), where a permeable

103   fault zone at more than 100 meters depth is able to provide about 100 m^3/h according to air-lift flow

104   measurements.

105   We first describe the characteristics of the groundwater system under ambient conditions to

106   highlight the hydrologic functioning of deep structures at the catchment scale. We then describe a 9-

107   week large-scale pumping test that was carried out to identify the hydraulic properties of the aquifer

108   system. During this test, various complementary experiments and measurements were conducted to

109   investigate flow interactions between the different reservoirs and to identify mixing processes.

110   Finally, the combined analyses from this multidisciplinary experiment are used to develop a

111   hydrogeological conceptual model of a sub-vertical fault zone in crystalline context.

112   2   GEOLOGICAL AND HYDROGEOLOGICAL SETTING

113   The experimental site of Saint-Brice en Coglès is located in the Mancellian Domain of the "*Massif*

114   *Armoricain"*, in Brittany (France), where it constitutes the north western French part of the

115   Cadomian and Variscan orogenies ((Figure 1a). This formation outcrops from western to central

116   Europe and is mainly composed of low to high grade (migmatite) metamorphic rocks, with regional-

117 scale magmatic intrusions (Cadomian granodiorites). The Mancellian Domain is limited in the north

118 by the English Channel, and to the south by the North Armorican Shear Zone (NASZ). The main

119 lithologies encountered are Precambrian (Brioverian) sedimentary rocks ((Figure 1a), composed of

120 alternating series of argillites/siltites and sandstones. These sedimentary rocks have been affected by

121 low grade metamorphism which has formed a metamorphic aureole around the Cadomian

122 granodiorites on a regional-scale (Ballèvre et al., 2009; Brun et al., 2001; Chantraine et al., 2001;

123 Cogné and Wright, 1980). The most important deformation zone corresponds to a major ESE-WNW

124 dextral strike-slip shear zone, the NASZ attributed to hercynian orogeny. Secondary SW-NE reverse

125 faults are also found around this main shear zone. These terrains have been affected by Pyrenean

126 and Alpine orogenies that have generated a diffuse deformation characterized by half-graben basins

127 (Rennes basin, Landéan basin…) and NW-SE sub-vertical faults (Grellet et al., 1993; Van Vliet-Lanoë et

128 al., 1997).

129 The Saint-Brice en Coglès site is located in the epimetamorphism zone of a large Cadomian pluton

130 (Fougère granite). The rocks consist of Brioverian sediments metamorphosed into hornfels schists.

131 The vicinity of the site is characterized by parallel extensional N-S normal faults that form localized

132 extensional basins (Geological map, BRGM (Dadet et al., 1984), (Figure 1b).

133 *(Figure 1)*

134 Local geological structures were imaged by carrying out a structural analysis including landscape,

135 geological mapping and geophysical (electric and seismic tomographies) analysis. Sub-vertical faults

136 and extensional graben structures were clearly identified ((Figure 2a). In addition, three deep

137 boreholes (MFT20, MFT80 and, F3) were drilled using "Down Hole Air Hammer" drilling method.

138 Another deep borehole (FC4, 250 m), which has been entirely cored, has been drilled along a profile

139 perpendicular to the orientation of the main accident lineament (Figure 2b). The borehole

140 characteristics are detailed in (Table 1. Several shallow boreholes (labeled T in (Figure 2b) were also

141 drilled to characterize the shallow weathered compartment. The first 10 meters contained highly

142 weathered material with high clay and sand contents. Examination of the cores revealed that the

143 Brioverian rocks were highly deformed and fractured, and intruded by metric aplites, pegmatites and

144 quartz veins, oriented N 50° to N 70°. Particularly, in the vicinity of the fault outcropping, the

145 Brioverian rocks are affected by horizontal fractures, characterized by a density decrease with depth,

146 to an average of about 40-50 meters. The main fault zone was identified in each borehole as a highly

147 fractured and productive zone, ranging from a few meters thick (see core sampling in (Figure 2c) to

148 15 m in the outcropping part of the borehole ((Table 1 and (Table 2). The fault typically dips by 70° to

149 the NNW ((Figure 2c). Wells were completed with a slotted casing in the deep productive zones.

150 *(Figure 2)*

151 *(Table 1)*

152 3 MATERIAL AND METHODS

153 3.1 FIELD EXPERIMENT

154 The interactions between the fault zone and the other hydrologic domains were described and

155 quantified by investigating the site under natural conditions and during a large-scale pumping test. A

156 packer was placed 80m below the ground surface in borehole F3 to ensure that pumping was carried

157 out deep within the fault zone. As a result, water abstraction occurred principally from the fault zone

158 at 110 meters below ground surface ((Table 1). Pumping lasted for two months (63 days) at a flow

159 rate of about 45 m³/h. During the pumping test, total rainfall was limited to 40 mm, and potential

160 evapotranspiration was 90 mm (information available from Saint Mars-sur-la-Futaie weather station-

161 48°26'N 0°58'W, 30km north-east of the Saint-Brice site). Complementary experiments and analyses

162 carried out are described in the following.

163 3.2 WATER LEVEL MONITORING AND ANALYSIS

7

164   Water levels were recorded using a pressure sensor with barometric compensation (STS© and

165   Schlumberger© pressure transmitters). The altitude of the well was determined by differential GPS.

166   The estimated uncertainty for the absolute water level measurements was about a centimeter. The

167   mean hydraulic parameters of the system under pumping conditions were determined from classic

168   analytical models. In addition, a logarithmic derivative method of drawdown measurement was used

169   to analyze flow regimes (Bourdet and Ayoub, 1989; Renard et al., 2008; Spane and Wurstner, 1993).

170   This method also permitted identification of flow behaviors and an estimation of the system's

171   transmissivity based on Cooper and Jacob's approximation (Renard et al., 2008).

172   3.3   HIGH RESOLUTION FLOW AND TEMPERATURE LOGGING

173   Structural heterogeneity of fractured rocks induces flow partitioning within the aquifer system. To

174   examine preferential flow path and fracture connectivity we used high-resolution flow logging (Heat

175   Pulse Flowmeter, Geovista©) under ambient and pumping conditions (Le Borgne et al., 2006b;

176   Paillet, 1998). Single-borehole flowmeter tests provide information on the main inflow or outflow

177   zones in a well and measure the prevailing ambient flow conditions in the absence of pumping (Le

178   Borgne et al., 2006b; Paillet, 1998). During a pumping test, cross-borehole flowmeter tests (pumping

179   in a given well and measurement in another) are based on the observation that transient flow during

180   pumping in a given aquifer modifies the hydraulic head distribution with time in the different

181   permeable domains and produces measurable changes in the vertical flow profiles. The connectivity

182   and hydraulic properties of the main flow paths can be identified by transitory flow measurements

183   (Le Borgne et al., 2006b; Paillet, 1998).

184   To define flow paths and origin of the water, temperature logging was also used with a multi-

185   parameter Hydrolab probe (OTT©) and Ocean seven 303 CTD (Idronaut©). Differences in hydraulic

186   heads between the fractures in a borehole, under ambient conditions or during pumping, will modify

187   the temperature profile with respect to the geothermic gradient. Therefore these temperature

188   profiles are very useful to identify hydraulic connections between compartments and their evolution

189   through time (Anderson, 2005; Bense et al., 2008; Chatelier et al., 2011).

190   3.4   TRACER TESTS

191   To identify transfer time distribution and to characterize groundwater flows within the main

192   transmissive fault zone, tracer tests were performed between observation wells and the pumped

193   borehole. Tracer breakthrough concentrations were monitored in the pumped well (F3) within the

194   upper casing and below the pump with a flow-through field fluorometer developed by the University

195   of Neuchâtel (Schnegg and Costa, 2007; Schnegg and Flynn, 2002). The fluorometers had been

196   previously calibrated with tracer and local fresh water in the laboratory. To optimize injection, we

197   identified the main fractured part of the fault zone connected to the pumped well (F3) in each

198   observation wells (MFT80 and FC4). Uranine tracer solution was injected in front of the main inflow

199   zone and we checked that no tracer solution remained in the borehole after the injection by logging

200   concentration through borehole depth.

201   3.5   GEOCHEMISTRY AND GROUNDWATER DATING

202   To identify water origin and estimate mixing processes, we analyzed geochemistry and groundwater

203   dating data under ambient and pumping conditions. The apparent ages of water samples were

204   determined by measuring Chlorofluorocarbons (CFCs) concentrations. These anthropogenic gases

205   provide information on groundwater resident times up to 50 years and can give information on

206   mixing processes between different water sources during flow changes   (Ayraud et al., 2008;

207   Busenberg and Plummer, 1992; Cook and Solomon, 1997; Cook et al., 2005; Jaunat et al., 2012).

208   Waters were sampled in stainless-steel ampoules after discarding at least three ampoule volumes,

209   and ensuring that there was no contact of the water with atmospheric gases.

210   Groundwater CFCs concentrations were measured by the Geosciences Rennes Laboratory (Labasque,

211   2006). Water samples were degassed by N2 stripping and then injected into a gas chromatograph

212   equipped with an electron capture detector (GC–ECD). The CFC concentration obtained by

213   chromatographic analysis was converted to the atmospheric mixing ratio (pptv – Parts per Trillion by

214   Volume) by applying a solubility function (modified Henry's Law for trace gases (Ayraud et al., 2008;

215   Bu and Warner, 1995; Warner and Weiss, 1985; Weiss and Price, 1980)). The CFC atmospheric mixing

216   ratios were then compared with the atmospheric evolution curve (Walker et al., 2000) to determine

217   the apparent recharge year, and thus the apparent age of the groundwater. Analytical uncertainty

218   for the CFC concentrations was estimated (Labasque, 2006) at around 3 % for recent water (<20

219   years) and 5 % for old water (between 55 to 30 years).

220   Major and trace elements were analyzed by ion chromatography (Dionex DX-100) and ICP-MS HP

221   4500 at the Geosciences Rennes Laboratory following standard laboratory methods. The analytical

222   uncertainty for major anions and cations was about 2%.

223   4   RESULTS

224   4.1   AMBIENT FLOW CONDITION

225   (Figure 3 shows the evolution of hydraulic head in the main boreholes representative of the

226   fractured domains (FC4, F3, MFT80 and MFT20) and in the upper weathered reservoir (T_i). The

227   seasonal evolution of hydraulic head is similar in all the aquifer system with a fast response to

228   rainfall during the recharge periods and a classic discharge regime observed during summer.

229   The hydraulic head gradient mostly follows the topography and indicates groundwater flow towards

230   the outcropping of the fault zone and discharge into the river (FC4-F3-MFT80 in (Figure 2b&c).

231   Measurements of the hydraulic gradient with depth revealed a higher hydraulic head in the deeper

232   boreholes ((Figure 3). This suggests a definite vertical compartmentalization of the aquifer system.

233   The three boreholes intersecting the permeable fault zone show similar hydraulic responses, with a

234   potential upward flow, according to the hydraulic gradient analysis. The MFT20 well, located at the

235   edge of the weathered and the fractured bed rock, remains under the influence of the fault zone.

236   The sub-surface aquifer situated within the upper weathered part (T_i boreholes), appears to be much

237   less influenced by the deep structure.

238   The fault domain responds quickly to rainfall even though it is locally covered by the sub-surface

239   reservoir with lower hydraulic head. This suggests that the bed rock domain can respond rapidly to

240   recharge. The recharge area is certainly along strike and up topographic gradient through favorable

241   deep fractured zones.

242   *(Figure 3)*

243   A typical variation of flow rate with depth is shown in (Figure 4. All flow profiles obtained under

244   ambient conditions reveal upward flow, implying that hydraulic head is higher in the deep fractures

245   (235m for FC4) than in the upper fractures (45m for FC4). FC4 profile in ambient conditions show a

246   major inflow zone at 245 m deep and a major outflow zone at 49 m deep (Figure 4). No other

247   contributing fractures can be detected, either because of the limit of detection of the tool, or simply

248   because of the lack of any hydraulic head gradient between the head in the fractures and the head in

249   the borehole. In pumping conditions, and for a much lower hydraulic head in the borehole, few

250   others fracture may be detected between 160 and 215 meters deep. In any case, the flow rate

251   profiles obtained under pumping conditions confirms that the deep conductive fault zone provides

252   about 50 to 75% of the total productivity of each borehole ((Table 2). For all profiles, the fracture

253   transmissivity was determined by using the model developed by Paillet (1998). The transmissivity of

254   the deep productive sections in each well appeared to be relatively high, ranging between 6 and 9 x

255   10^{-4} m²/s ((Table 2).

256   *(Table 2)*

257   Groundwater dating by CFCs analyses also highlighted the influence of an old deep water origin, with

258   tracer concentrations close to the detection limit in all deep boreholes ((Table 3), including the 20m

11

259   depth well. The apparent water age is older than 55 years. Conversely, CFCs analyses in the first 10 m

260   of the weathered domain revealed recent waters and contamination with nitrate. Globally, the

261   apparent age determined in the upper weathered reservoir and based on a piston flow model, is 20

262   years. Moreover, the water age in this upper part of the aquifer system decrease uphill. This suggests

263   that the subsurface aquifer is partially influenced by deep groundwater discharge (more or less 25%

264   of old deep water).

265   *(Table 3)*

266   To summarize, three main hydraulic domains were highlighted at the Saint-Brice site: (1) the fault

267   zone which has a higher transmissivity, (2) the surrounding domain affected by secondary fractures

268   less transmissive and (3) the upper weathered part of the aquifer system, restricted to the first 10

269   meters. Under ambient conditions, the hydrogeological system is clearly driven by the discharge

270   from a deep groundwater system towards the upper part of the aquifer system and the local stream.

271   *(Figure 4)*

272   4.2   PUMPING CONDITION

273   4.2.1   EVOLUTION OF HYDRAULIC HEADS AND DIAGNOSTIC PLOT

274   During the 60-days pumping experiment, the hydraulic heads in the different boreholes were

275   recorded ((Figure 5). All wells located in or near the sub-vertical fault zone, including the shallow

276   piezometers in the sub-surface weathered domain, reacted quickly to pumping. During the first 10

277   days, drawdown was limited to a few meters and was similar in all boreholes. This suggests a good

278   connection between the upper and lower domains of the aquifer system. After 10 days of pumping,

279   drawdown has exceeded the depth of the sub-surface wells (<10 m deep), due to desaturation of the

280   upper weathered reservoir around the pumping well. As observed in all deep boreholes, drawdown

281   increased significantly during the last 50 days of pumping ((Figure 5).

282   *(Figure 5)*

283   Figure 6 displays the normalized drawdown (s/Q) of pumping well F3 and its derivative through time

284   in a log-log diagram. The evolution of the derivative curve provides information on flow behaviors

285   and on boreholes effects such as wellbore storage and skyn effects. Such diagnostic curves can be

286   used to interpret different flow regimes (Bourdet et al., 1983; Renard et al., 2008), e.g. double

287   porosity, leakage effect, no-flows boundaries… Here, considering the specific geometry of the aquifer

288   system, we assumed that flow regimes can be described through a simple model developed for

289   fracture or strip aquifer embedded in lower permeable block (Butler and Liu, 1991; Escobar and

290   Hernández, 2010; Gringarten, 1996; Moench, 1984; Rafini and Larocque, 2009; Tiab, 2005). Such

291   fracture models involve generally three characteristic flow regimes: the early local response of the

292   fault zone, a period of transition controlled by the geometrical fault zone properties at larger scale

293   and finally the global hydraulic response of the system.

294   Flow behaviors can be detailed as follow through derivative description: ((Figure 6). 1) After the first

295   early-time where the drawdown response is influenced by wellbore storage and skin effects, a short

296   radial flow response is observed. This reflects the behavior of the local permeable fault zone, where

297   water was principally extracted from the local fracture storage and eventually fed by proximal matrix

298   storage and/or local leakage from overlaying aquifers. The constant derivative value suggests a

299   transmissivity around $10^{-3}\ m^2.s^{-1}$. The derivative decrease between 0.1 and 1 day can be the

300   consequence of preferential leaky flows from shallower reservoir. 2) Between 1 to 30 days of

301   pumping, the drawdown derivative curve is characterized by a transitory period with a strong

302   increase (derivative slope of ½). This derivative increase can be interpreted as double porosity

303   behavior for which lateral inflows from surrounding reservoirs supply the permeable fault at larger

304   scale. The fault geometry can also influence the drawdown during this transitory period which

305   induces linear flow regime. 3) Finally, the system reached a radial flow condition during the last

306   month of pumping, where the whole system was solicited indicating that the major flow comes from

307   surrounding low-permeability domains (Butler and Liu, 1991). The normalized constant derivative of

308 0.18 m at the end of the test implies a global transmissivity of the aquifer system about

309 $10^{-4}\,m^2.s^{-1}$.

310 *(Figure 6)*

311 4.2.2 FLOWMETER TEST AND TEMPERATURE LOGGING

312 Flow and temperature logs under natural and pumping conditions are presented for MFT80 in (Figure

313 7. Other observation wells yielded similar results. Under ambient conditions, upward flows were

314 identified ((Figure 7 a_1), implying that the hydraulic head in the deeper part of the fault zone was

315 higher than in the upper part of the aquifer domain. During pumping, downward flows were

316 measured, indicating a greater decrease of the hydraulic head in the fault zone. Downward flow

317 could be even 3 times greater than the previous upward flow, which implied a clear inversion of flow

318 between the hydraulic permeable domains ((Figure 7 b_1). Nevertheless, the downward borehole

319 flows slowed down after a few days, in conjunction with the decrease in head gradient between the

320 two compartments ((Figure 7 c_1).

321 Temperature logs ((Figure 7_2), carried out under ambient conditions and during pumping in all

322 observation wells, showed a clear temperature decrease of about 0.2 to 1°C with pumping. The

323 homogeneity of the profiles, with lower temperatures than under ambient conditions, suggests that

324 the deep aquifer domain was fed by colder water coming from the sub-surface domain ((Figure 7 b_2

325 and c_2). This confirms that pumping is initiated within the fault zone at depth and that the upper

326 aquifer domain is supplying the deeper structure.

327 *(Figure 7)*

328 4.2.3 PUMPING TEST MODELING

329 The hydraulic parameters of the aquifer system were evaluated by fitting the drawdown data with

330 classic analytical models. Different solutions were applied to interpret the dataset at different times

331 ((Figure 8). in view to characterize the two main flow behaviors involved during the test, previously

14

332   characterized by the derivative interpretation: 1) the fault storage response, supported by leaky flow

333   from the weathered part of the aquifer system (<10 days of pumping) and 2) the global double

334   porosity response of the aquifer system during long term pumping.

335   For the first 10 days of pumping, the double porosity analytical solution according to Moench's

336   model (Moench, 1984) was used to model the local fault zone response. This model is based on the

337   concept of a fracture embedded within blocks of lower permeability, characterized by matrix

338   storage. Solutions are presented in equations 19 and 20 from the Moench paper of 1984 and plotted

339   for the early time in MFT80 for both drawdown and its derivative in (Figure 8a. Quadratic head losses

340   were estimated by a variable rate pumping test at 2.5 10^4 m^{-5}s^2. Hydraulic parameters deduced from

341   all wells are listed in (Table 4. These parameters confirm that, during the first days of pumping, flow

342   is controlled by a relatively high transmissive ($T1 = 7.10^{-4}m^2.s^{-1}$) fault zone embedded in lower

343   permeability blocks ($Kb = 2.10^{-8}m.s^{-1}$). A strong fracture skin value (set to 1) was required to

344   model the first times of both drawdown and derivative, which suggest a strong delay contribution

345   between surrounding blocks to the fractured zone (Moench, 1984).

346   *(Table 4)*

347   We also used the "Two Aquifer-System" model developed by Hunt and Scott (2007) to characterize

348   drainage flows from weathered reservoir to the fractured domain. This model assumes a screened

349   well in an aquifer overlain by an aquitard and an unconfined aquifer which may represent here the

350   upper weathered reservoir. A mean transmissivity of $T1 = 5.10^{-4}m^2.s^{-1}$ for the deeper aquifer

351   domain, and transmissivity and porosity estimates of $6.10^{-5}m^2.s^{-1}$ and 2% respectively, for the

352   superficial aquifer was required to fit both drawdowns and derivatives (plot in (Figure 8a, results in

353   (Table 4).

354   For modeling the hydraulic behavior of the hydrological system at global scale after the first 8 hours

355   of pumping, Moench's model (Moench, 1984) proved to be the simplest and most efficient model to

356   reproduce the data ((Figure 8b). The estimated transmissivity of the fractured system is $T1 =$

357 $10^{-4} m^2.s^{-1}$, embedded within a reservoir (matrix) with a lower permeability of $Kb = 2.10^{-8} m.s^{-1}$

358 and a relatively high specific storage of $Sb = 10^{-3}\ m^{-1}$. A high value of fracture skin is still necessary

359 to reproduce the transitory flow regime observed during transitory pumping times (Figure 6). The

360 transmissivity deduced for long times pumping tends to the transmissivity of the global permeable

361 system (Butler and Liu, 1991).

362 Note that the estimation of storativity in adjacent blocks based on Moench's model is relatively large.

363 However, storativity is in general difficult to estimate in heterogeneous crystalline rocks (Burbey,

364 2003; Le Borgne et al., 2006a; Meier et al., 1998; Neuman, 1979). This higher value may also reflect

365 the fact that only two main compartments (fracture and matrix) were used in the model, whereas

366 several capacitive domains, including a superficial one in the weathered rocks, may actually be

367 involved in the response to pumping.

368 *(Figure 8)*

369 4.2.4 GEOCHEMISTRY AND GROUNDWATER DATING

370 Chemical analyses of major ions revealed Ca-Mg-CO$_3$ in water from the fault zone and Ca-Mg-CO$_3$

371 SO$_4$-Cl, characteristic of anthropogenic activities, in water from the shallower weathered domain. A

372 clear evolution of groundwater chemistry was observed during pumping, due to the mixing of water

373 of different origins. In particular, mixing with the upper weathered reservoir was clearly apparent

374 during the first ten days of pumping. The geochemical response after a longer period was dependent

375 both on shallower and "matrix" contributions and modified by reactivity processes. Description of

376 geochemical evolution will require a much more detailed analysis and will be published in another

377 article (Roques et al., "In Preparation"). Our main focus here is to highlight changes in the apparent

378 age of groundwater, using conservative anthropogenic tracers such as CFCs to highlight the mixing

379 processes.

380   The evolution of groundwater apparent age was deduced from the CFC-12 and CFC-113

381   concentrations in samples taken at the pumping wellhead (

382   (Figure 9). An asymptotic increase in CFCs concentrations was observed, implying a decrease in

383   apparent age, given the assumption of a piston flow model. Under ambient conditions, the CFCs

384   concentrations in the F3 well were negligible, close to the measurement uncertainty, and

385   characteristic of an apparent age exceeding 55 years. After 60 days of pumping, the mean apparent

386   age of water sampled at the outflow was about 40 years. This clearly confirms the influence of the

387   recent water solicited during pumping. Since old water was found in most of the boreholes, this

388   recent water must come from the upper weathered aquifer (<10m). The result also confirms the

389   relatively fast transfer time between compartments.

390   *(Figure 9)*

391   The contribution of the weathered aquifer may easily be estimated by considering a simple binary

392   mixing assumption. We first assumed that mixing occurred between i) water of high apparent age

393   i.e., 55 years (CFC12 concentrations of 0 to 50 pptv) the representative signature of deep fault water,

394   and ii) water from the upper weathered compartment with a mean apparent age of 20 years (CFC12

395   concentrations of 550 pptv measured in the superficial boreholes before pumping). Based on these

396   assumptions, the estimated contribution of the upper weathered aquifer was around 15-20% at the

397   end of pumping (last 30 days, CFC concentration = 105 pptv).

398   These observations clearly demonstrate that the superficial compartment contributes to the global

399   mixing process when the deep fault zone aquifer is pumped. It is difficult to clearly define the

400   contribution of each compartment without a detailed analysis of the mixing process (Roques et al., in

401   preparation), which is beyond the scope of the present work. However, both the geochemistry

402   evolution and groundwater dating suggest that after one month of pumping about 20% of the

403   pumped water comes from the upper part of the aquifer system.

404   4.2.5 TRACER TESTS

405   Two tracer tests were performed during pumping. Uranine tracer was injected in the main

406   productive fault zone in two observation wells: MFT80 and FC4 at 55 and 235 meters depth

407   respectively. (Figure 10 displays the evolution of normalized concentrations with time for the two

408   breakthrough curves. In the first tracer test (MFT80 towards F3), the tracer was detected 4 hours

409   after injection while the maximum concentration occurred at about 16 hours. The estimated travel

410   distance between the injection point in MFT80 and the main inflow zone in F3 was around 53 meters,

411   implying an average flow velocity of about 3.3 m/h. In the second test (FC4 to F3), the tracer

412   appeared 20 hours after injection and the peak concentration was apparent after about 220h. A

413   slight double peak was observed, certainly due to different flow paths between the two wells. Taking

414   into account a travel distance of about 135m, the estimated average flow velocity in the deep

415   structure was 0.6 m/h, i.e. 5.5 times slower than in the upper part of the fault zone. This implies

416   either that the Darcy velocities were much lower in the deeper compartment or that porosity in the

417   deeper compartment was much higher.

418   The Becker and Charbeneau (2000) solution for converging radial flow was used to compute the

419   present breackthrough curves (Figure 10). The use of this model is justified for highly dispersive

420   system like this one (Peclet number are around 5, where Pe = R/α, with R is the travel distance and α

421   the dispersivity). The modeling objectives are to derive first order transport parameters and to

422   estimate roughly flow partitioning within the permeable fault zone ((Figure 10). The modeling was

423   achieved by setting the injected mass to the restitution rate (around 85% for MFT80 and 45% for

424   FC4). It was not possible to use the same set of parameters to fit the two breakthrough curves

425   ((Figure 10). Firstly, dispersivity was apparently two times higher during the deeper tracer test (FC4).

426   This increase in dispersivity can be explained by a scaling effect that is classically observed in large

427   scale tracer tests (Gelhar, 1992) and due to the integration of heterogeneities along pathways.

428   Secondly, fitting both curves would require either constant flow rates or constant parameters for the

429   fault zone (thickness and porosity). Assuming an average fault thickness of 6 meters and a constant

430   porosity of around 1 to 2% we were able to obtain a relatively good match for both breackthrough

431   curves ((Figure 10). Porosity values obtained in this case appears relatively high for crystalline rocks,

432   but still reasonable, considering FC4 cores samples (Figure 2), which show that the productive zones

433   are highly fractured and open. The difference in restitution time between the two tracer tests could

434   be honored in this case only by using different effective flowrates for the two tracer tests. This

435   interpretation would imply that the flow-rate from the upper of the aquifer system represented

436   about 2/3 of the total pumping rate while the flow rate from the deeper part was limited to the

437   other 1/3.

438   Note that the difference in restitution time could be similarly modeled by assuming a permeability

439   decrease with depth or a porosity increase with depth. However, an increase of porosity with depth

440   would be difficult to explain, and permeability, as deduced from previous single borehole tests,

441   appears to remain relatively constant with fault deepening ((Table 2). Such differences may be also

442   partly the results of fault zone heterogeneities. Nevertheless, in both cases tracer injection were

443   done in fractured zone of similar local permeability values. It therefore seems more reasonable to

444   model both tracer tests by assuming flow partitioning through depth.

445   *(Figure 10)*

446

447 5 DISCUSSION: CONCEPTUAL MODEL

448 The results obtained in the previous sections were synthesized to derive a global conceptual model

449 of the Saint-Brice en Coglès aquifer system. Our aim was to describe the hydraulic functioning of this

450 steep fault zone under ambient and pumping conditions, and to estimate the groundwater resources

451 actually available.

452 5.1 SUB-VERTICAL STRUCTURE PROPERTIES AND IMPACT ON GROUNDWATER FLOW

453 The main permeable structure has developed along an extensive normal fault zone. Boreholes at

454 different depth (MFT80, F3 and FC4) were used to investigate the fault zone properties. The fault

455 permeability appears relatively constant with depth and constitutes a sub-vertical strip fractured

456 zone embedded in low-permeability domains and overlain by a weathered horizontal unconfined

457 domain which does not exceed 10 meters depth (T$_i$ piezometers).

458 Various complementary approaches were used to characterize the discharge of deep groundwater

459 through the sub-vertical permeable fault zone. Geochemistry and groundwater dating indicated the

460 presence of an old water signature in the fractured domain from 250 to 20m. As the hydraulic heads

461 in the deeper part are higher, the deep water finds a preferential flow path along the permeable

462 fault zone and is discharged towards the subsurface aquifer domains in the watershed outlet (*(Figure*

463 *11*a). Fluxes from the deeper part of the aquifer system can be quantified from the fault zone

464 permeability deduced from hydraulic tests and the mean hydraulic gradient between the deep and

465 subsurface domain. Assuming that the flowrate is constant along the length of the fault (about

466 1000m deduced from the estimated lineament length), the discharge ranges between 170 and

467 200 m^3/day. Although this amount of natural flux along fault zones is significant, it is generally poorly

468 known, and is not usually considered in the local hydrogeological balance.

469 *(Figure 11)*

470   5.2 FLOW BEHAVIOR AND RELATIONSHIPS BETWEEN COMPARTMENTS UNDER PUMPING

471   CONDITIONS

472   A multi-disciplinary approach was adopted to investigate flow behavior and water exchanges

473   between the different aquifer domains which enabled us to derive a conceptual model of the

474   hydraulic behavior of this deep permeable fault zone.

475   The most relevant observation is that the sub-vertical fault is clearly connected with the sub-surface

476   reservoir and the two compartments are therefore highly dependent on each other. Globally,

477   pumping in the deep structure induces downward groundwater flow from the upper aquifer domain

478   (*(Figure 11*b). Due to the limited storage in the fault zone, water fluxes during pumping are mainly

479   supported by the overlaying reservoir and/or adjacent domains. After two months of water

480   extraction, it is clear that pumping involves contributions from the surrounding compartments, which

481   implies sub-surface and lateral inflows (matrix storage) towards the sub-vertical structure. Tracer test

482   analyses showed that about 2/3 of the water flow originates from the upper part of the aquifer

483   system. This partition of fluxes seems to be governed mainly by hydraulic boundary conditions which

484   limit the deep supply during pumping. As a result, the superficial part of the aquifer seems to

485   constitute a key reservoir supplying the faulted bedrock domain during pumping. The lateral

486   influence of pumping seems to be limited to 300 meters from the fault, as observed in some

487   subsurface boreholes. Thus, in the case of a fault with a large dip (approximately 70°) and a high

488   permeability contrast with surrounding compartments, the radial expansion of the drawdown and

489   pressure variation is preferentially transferred along the fault zone. In the present case, pressure

490   variations diffuse mainly along the graben structure, in the lower topographic zone where the

491   wetland has developed (*(Figure 11*b). This behavior implies that fault zones, when they are

492   permeable, may allow pressure diffusion along the fault plane that can act almost as a boundary

493   condition to drain groundwater from the surrounding reservoirs. Similar behavior has been described

494   through numerical modeling of groundwater flow in fault zones (Leray et al., 2013).

495   21

496 CONCLUSIONS

497   In this study, we used a multidisciplinary approach to investigate the hydrogeologic behavior of a

498   sub-vertical permeable fault and quantify its interactions with surrounding reservoirs, under ambient

499   and pumping conditions. This study provides a good example of the functioning of a sub-vertical fault

500   determined from lineament mapping.

501   Our results suggest that sub-vertical fault and sub-surface reservoirs are highly dependent on each

502   other. Under ambient conditions, the fault allows the discharge of regional old water into superficial

503   aquifer domains. The natural discharge rate of the fault zone is estimated to be around 170 to 200

504   m^3/day. Although relatively low, this value should be taken into account when estimating water

505   fluxes, hydrologic budget and solute transport at the watershed scale. During the early stages of

506   pumping, the hydrological system is strongly dependent on storage from the sub-surface weathered

507   reservoir. Once the upper weathered reservoir has become mainly unsaturated, the system acts as a

508   classic dual porosity medium with a highly transmissive structure embedded in lower permeable

509   compartments. Thus, this high permeability fault zone appears to be an efficient thin permeable

510   domain that permits rapid diffusion of pressure but is strongly dependent on sub-surface and

511   adjacent domains of higher storativity. All field measurements suggest that under pumping

512   conditions, most of the flow comes from superficial domains and from the vicinity of the fault zone,

513   with a recharge area located at the surface mainly along the fault zone. Moreover, such steep fault

514   zones, although of relatively high transmissivity, remain relatively limited in terms of groundwater

515   yield. In this study, the pumping test was carried out for 2 months at a flow-rate of 45 m^3/h, but the

516   piezometric analysis indicates that this rate was certainly too high to be sustainable. A better

517   estimate of sustainable flowrate would be around 20 to 30 m^3/h. This is a much lower value than

518   some other fault zone aquifers, such as gently dipping fault zones which may provide higher

519   groundwater resources (Le Borgne et al., 2006a; Ruelleu et al., 2010). This difference confirms the

520   role of the dip of the fault-zone that may greatly increase borehole yield in some circumstances

521   (Leray et al., 2013).

522   **Acknowledgments**

534

535 REFERENCES

536 Amiotte Suchet, P., Probst, J.-L., Ludwig, W., 2003. Worldwide distribution of continental
537   rock lithology: Implications for the atmospheric/soil CO_2 uptake by continental
538   weathering and alkalinity river transport to the oceans. Global Biogeochem. Cycles 17,
539   1–13.

540 Anderson, E.I., Bakker, M., 2008. Groundwater flow through anisotropic fault zones in
541   multiaquifer systems. Water Resour. Res. 44, 1–11.

542 Anderson, M.P., 2005. Heat as a ground water tracer. Ground Water 43, 951–68.

543 Apaydin, A., 2010. Relation of tectonic structure to groundwater flow in the Beypazari region,
544   NW Anatolia, Turkey. Hydrogeol. J. 18, 1343–1356.

545 Aydin, A., 2000. Fractures, faults, and hydrocarbon entrapment, migration and flow. Mar. Pet.
546   Geol. 17, 797–814.

547 Ayraud, V., Aquilina, L., Labasque, T., Pauwels, H., Molenat, J., Pierson-Wickmann, A.-C.,
548   Durand, V., Bour, O., Tarits, C., Le Corre, P., 2008. Compartmentalization of physical
549   and chemical properties in hard-rock aquifers deduced from chemical and groundwater
550   age analyses. Appl. Geochemistry 23, 2686–2707.

551 Bahat, D., 1999. Mechanism of exfoliation joint formation in granitic rocks, Yosemite National
552   Park. J. Struct. Geol. 21, 85–96.

553 Ballèvre, M., Bosse, V., Ducassou, C., Pitra, P., 2009. Palaeozoic history of the Armorican
554   Massif: Models for the tectonic evolution of the suture zones. Comptes Rendus Geosci.
555   341, 174–201.

556 Banwart, S., Gustafsson, E., Laaksoharju, M., 1994. Fracture zone in crystalline bedrock:
557   Initial hydrochemical perturbation during tunnel construction at the Äspö Hard Rock
558   Laboratory, southeastern Sweden. Water Resour. Res. 30, 1747–1763.

559 Becker, M.W., Charbeneau, R., 2000. First-passage-time transfer functions for groundwater
560   tracer tests conducted in radially convergent flow. J. Contam. Hydrol. 40, 299–310.

561 Bense, V.F., Person, M. a., 2006. Faults as conduit-barrier systems to fluid flow in siliciclastic
562   sedimentary aquifers. Water Resour. Res. 42, 1–18.

563 Bense, V.F., Person, M. a., Chaudhary, K., You, Y., Cremer, N., Simon, S., 2008. Thermal
564   anomalies indicate preferential flow along faults in unconsolidated sedimentary aquifers.
565   Geophys. Res. Lett. 35, 1–6.

566 Bense, V.F., Van den Berg, E.H., Van Balen, R.T., 2003. Deformation mechanisms and
567   hydraulic properties of fault zones in unconsolidated sediments; the Roer Valley Rift
568   System, The Netherlands. Hydrogeol. J. 11, 319–332.

569 Blatt, H., Jones, R., 1975. Proportions of exposed igneous, metamorphic, and sedimentary
570   rocks. Geol. Soc. Am. Bull. 86, 1085–1088.

571 Bourdet, D., Ayoub, J., 1989. Use of pressure derivative in well test interpretation. SPE
572   Form. Eval. 4, 293–302.

573 Bourdet, D., Whittle, T., Douglas, A., Pirard, Y., 1983. A new set of type curves simplifies well
574   test analysis. World Oil 196, 95–106.

575 Boutt, D.F., Diggins, P., Mabee, S., 2010. A field study (Massachusetts, USA) of the factors
576   controlling the depth of groundwater flow systems in crystalline fractured-rock terrain.
577   Hydrogeol. J. 18, 1839–1854.

578 Brun, J.-P., Guennoc, P., Truffert, C., Vairon, J., 2001. Cadomian tectonics in northern
579   Brittany: a contribution of 3-D crustal-scale modelling. Tectonophysics 331, 229–246.

580 Bu, X., Warner, M.J., 1995. Solubility of chlorofluorocarbon 113 in water and seawater. Deep
581   Sea Res. Part I Oceanogr. Res. Pap. 42, 1151–1161.

582 Burbey, T.., 2003. Use of time–subsidence data during pumping to characterize specific
583   storage and hydraulic conductivity of semi-confining units. J. Hydrol. 281, 3–22.

584 Busenberg, E., Plummer, L.N., 1992. Use of chlorofluorocarbons (CCl3F and CCl F2) as
585   hydrologic tracers and age-dating tools: The alluvium and terrace system of central
586   Oklahoma. Water Resour. Res. 28, 2257–2283.

587 Butler, J.J., Liu, W.Z., 1991. Pumping tests in non-uniform aquifers: the linear strip case. J.
588   Hydrol. 128, 69–99.

589 Caine, J., Evans, J., Forster, C., 1996. Fault zone architecture and permeability structure.
590   Geology 24, 1025–1028.

591 Caine, J.S., Tomusiak, S.R.A., 2003. Brittle structures and their role in controlling porosity
592   and permeability in a complex Precambrian crystalline-rock aquifer system in the
593   Colorado Rocky Mountain Front Range. GSA Bull. 115, 1410–1424.

594 Carn-Dheilly, A., Thomas, E., 2008. RAPSODI - Recherche d'aquifères profonds dans le
595   socle du département de l'Ille et Vilaine. Rapport Final - BRGM/RP-56749-FR.

596 Carucci, V., Petitta, M., Aravena, R., 2012. Interaction between shallow and deep aquifers in
597   the Tivoli Plain (Central Italy) enhanced by groundwater extraction: A multi-isotope
598   approach and geochemical modeling. Appl. Geochemistry 27, 266–280.

599 Chantraine, J., Egal, E., Thiéblemont, D., Le Goff, E., Guerrot, C., Ballèvre, M., Guennoc, P.,
600   2001. The Cadomian active margin (North Armorican Massif, France): a segment of the
601   North Atlantic Panafrican belt. Tectonophysics 331, 1–18.

602 Chatelier, M., Ruelleu, S., Bour, O., Porel, G., Delay, F., 2011. Combined fluid temperature
603   and flow logging for the characterization of hydraulic structure in a fractured karst
604   aquifer. J. Hydrol. 400, 377–386.

605 Chilton, P.J., Foster, S.D.S., 1995. Hydrogeological characterization and water-supply
606   potential of basement aquifers in tropical Africa. Hydrogeol. J. 3, 36–49.

607   Cogné, J., Wright, A.E., 1980. L'orogène Cadomien – Geology of Europe from Precambrian
608   to the post-Hercynian sedimentary basins. 26th Int. Geol. Congr. – BRGM Mem 108,
609   29–55.

610   Cook, P., Love, a, Robinson, N., Simmons, C., 2005. Groundwater ages in fractured rock
611   aquifers. J. Hydrol. 308, 284–301.

612   Cook, P., Solomon, D., 1997. Recent advances in dating young groundwater:
613   chlorofluorocarbons, 3H/3He and 85Kr. J. Hydrol. 191, 245–265.

614   Dadet, P., Beurrier, M., Lautridou, J.-P., 1984. Notice explicative de la feuille Saint-Hilaire-
615   Du-Harcouët à 1/50 000. BRGM, Orléans.

616   Dewandel, B., Lachassagne, P., Wyns, R., Maréchal, J.C., Krishnamurthy, N.S., 2006. A
617   generalized 3-D geological and hydrogeological conceptual model of granite aquifers
618   controlled by single or multiphase weathering. J. Hydrol. 330, 260–284.

619   Escobar, F.H., Hernández, D.P., 2010. Pressure and pressure derivative analysis for long
620   naturally fractured reservoirs using the TDS technique. DYNA 77, 102–114.

621   Evans, J.P., Forster, C.B., Goddard, J. V., 1997. Permeability of fault-related rocks, and
622   implications for hydraulic structure of fault zones. J. Struct. Geol. 19, 1393–1404.

623   Fernandes, A., Rudolph, D., 2001. The influence of Cenozoic tectonics on the groundwater-
624   production capacity of fractured zones: a case study in Sao Paulo, Brazil. Hydrogeol. J.
625   9, 151–167.

626   Folch, A., Mas-Pla, J., 2008. Hydrogeological interactions between fault zones and alluvial
627   aquifers in regional flow systems. Hydrol. Process. 22, 3476–3487.

628   Ganerod, G.V., Braathen, A., Willemoes-Wissing, B., 2008. Predictive permeability model of
629   extensional faults in crystalline and metamorphic rocks; verification by pre-grouting in
630   two sub-sea tunnels, Norway. J. Struct. Geol. 30, 993–1004.

631   Gannon, J.P., Burbey, T.J., Bodnar, R.J., Aylor, J., 2011. Geophysical and geochemical
632   characterization of the groundwater system and the role of Chatham Fault in
633   groundwater movement at the Coles Hill uranium deposit, Virginia, USA. Hydrogeol. J.
634   20, 45–60.

635   Gelhar, L., 1992. A critical review of data on field-scale dispersion in aquifers. Water Resour.
636   Res. 28, 1955–1974.

637   Gleeson, T., Novakowski, K., 2009. Identifying watershed-scale barriers to groundwater flow:
638   Lineaments in the Canadian Shield. Geol. Soc. Am. Bull. 121, 333–347.

639   Goddard, J. V., Evans, J.P., 1995. Chemical changes and fluid-rock interaction in faults of
640   crystalline thrust sheets, northwestern Wyoming, U.S.A. J. Struct. Geol. 17, 533–547.

641   Grellet, B., Combes, P., Granier, T., Philip, H., 1993. Sismotectonique de la France
642   métropolitaine dans son cadre géologique et géophysique. Mem. N.S. SGF 164 1-2.

643   Gringarten, E., 1996. 3-D geometric description of fractured reservoirs. Math. Geol. 28, 881–
644   893.

645   Harte, P., Robinson, G., Ayotte, J., Flanagan, S., 2008. Framework for Evaluating Water
646   Quality of the New England Crystalline Rock Aquifers. U.S. Geol. Surv. Open-File Rep.
647   2008–1282 47.

648   Henriksen, H., Braathen, A., 2005. Effects of fracture lineaments and in-situ rock stresses on
649   groundwater flow in hard rocks: a case study from Sunnfjord, western Norway.
650   Hydrogeol. J. 14, 444–461.

651   Holland, M., Witthüser, K.T., 2011. Evaluation of geologic and geomorphologic influences on
652   borehole productivity in crystalline bedrock aquifers of Limpopo Province, South Africa.
653   Hydrogeol. J. 19, 1065–1083.

654   Hunt, B., Scott, D., 2007. Flow to a Well in a Two-Aquifer System. J. Hydrol. Eng. 12, 146–
655   155.

656   Jaunat, J., Huneau, F., Dupuy, A., Celle-Jeanton, H., Vergnaud-Ayraud, V., Aquilina, L.,
657   Labasque, T., Le Coustumer, P., 2012. Hydrochemical data and groundwater dating to
658   infer differential flowpaths through weathered profiles of a fractured aquifer. Appl.
659   Geochemistry 27, 2053–2067.

660   Labasque, T., 2006. Analyse des CFC dans les eaux souterraines. Géosciences Rennes,
661   Cahiers techniques de Géosciences Rennes, Rennes.

662   Le Borgne, T., Bour, O., Paillet, F., Caudal, J., 2006a. Assessment of preferential flow path
663   connectivity and hydraulic properties at single-borehole and cross-borehole scales in a
664   fractured aquifer. J. Hydrol. 328, 347–359.

665   Le Borgne, T., Paillet, F., Bour, O., Caudal, J.-P., 2006b. Cross-borehole flowmeter tests for
666   transient heads in heterogeneous aquifers. Ground Water 44, 444–52.

667   Leray, S., de Dreuzy, J.-R., Bour, O., Bresciani, E., 2013. Numerical modeling of the
668   productivity of vertical to shallowly dipping fractured zones in crystalline rocks. J. Hydrol.
669   481, 64–75.

670   Maréchal, J., Wyns, R., 2004. Vertical anisotropy of hydraulic conductivity in the fissured
671   layer of hard-rock aquifers due to the geological structure of weathering profiles. J.
672   Geol. Soc. India 5, 545–550.

673   Meier, P.M., Carrera, J., Sánchez-Vila, X., 1998. An evaluation of Jacob's Method for the
674   interpretation of pumping tests in heterogeneous formations. Water Resour. Res. 34,
675   1011–1025.

676   Melchiorre, E.B., Criss, R.E., Davisson, M.L., 1999. Relationship between seismicity and
677   subsurface fluids, central Coast Ranges, California. J. Geophys. Res. 104, 921–939.

678   Moench, F., 1984. Double-Porosity Models for a Fissured Groundwater Reservoir With
679   Fracture Skin. Water Ressources Res. 20, 831–846.

680   Neuman, S.P., 1979. Perspective on "Delayed yield". Water Resour. Res. 15, 899–908.

681   Paillet, F.L., 1998. Flow modeling and permeability estimation using borehole flow logs in
682   heterogeneous fractured formations. Water Resour. Res. 34, 997–1010.

683 Rafini, S., Larocque, M., 2009. Insights from numerical modeling on the hydrodynamics of
684   non-radial flow in faulted media. Adv. Water Resour. 32, 1170–1179.

685 Renard, P., Glenz, D., Mejias, M., 2008. Understanding diagnostic plots for well-test
686   interpretation. Hydrogeol. J. 17, 589–600.

687 Richard, B., Moore, B., Schwarz, G.E., Clark, S.F., Walsh, G.J., Degnan, J.R., 2002. Factors
688   Related to Well Yield in the Fractured-Bedrock Aquifer of New Hampshire. U.S. Geol.
689   Surv. Prof. Pap. 1660, 1–51.

690 Ruelleu, S., Moreau, F., Bour, O., Gapais, D., Martelet, G., 2010. Impact of gently dipping
691   discontinuities on basement aquifer recharge: An example from Ploemeur (Brittany,
692   France). J. Appl. Geophys. 70, 161–168.

693 Sander, P., 2006. Lineaments in groundwater exploration: a review of applications and
694   limitations. Hydrogeol. J. 15, 71–74.

695 Schnegg, P., Costa, R., 2007. Tracer tests made easier with field fluorometers. Bull.
696   d'Hydrogéologie 20, 20–21.

697 Schnegg, P., Flynn, R., 2002. Online field fluorometers for hydrogeological tracer tests. Isot.
698   und Tracer der Wasserforschung, Tech. Univ. Bergakademie Freiberg,
699   Wissenschaftliche Mitteilungen, Inst. für Geol. 19, 29–36.

700 Singhal, B., Gupta, R., 2010. Applied Hydrogeology of Fractured Rocks: Second Edition.
701   Springer.

702 Sophocleous, M., 2002. Interactions between groundwater and surface water: the state of
703   the science. Hydrogeol. J. 10, 52–67.

704 Spane, F., Wurstner, S., 1993. DERIV: A computer program for calculating pressure
705   derivatives for use in hydraulic test analysis. Ground Water 31, 814–822.

706 Stober, I., Bucher, K., 1999. Deep groundwater in the crystalline basement of the Black
707   Forest region. Appl. Geochemistry 14, 237–254.

708 Taylor, R., Howard, K., 2002. A tectono-geomorphic model of the hydrogeology of deeply
709   weathered crystalline rock: Evidence from Uganda. Hydrogeol. J. 8, 279–294.

710 Taylor, R.G., Howard, K.W.F., 1999. Lithological evidence for the evolution of weathered
711   mantles in Uganda by tectonically controlled cycles of deep weathering and stripping.
712   CATENA 35, 65–94.

713 Tiab, D., 2005. Analysis of pressure derivative data of hydraulically fractured wells by the
714   Tiab's Direct Synthesis technique. J. Pet. Sci. Eng. 49, 1–21.

715 Van Vliet-Lanoë, B., Bonnet, S., Hallegouët, M., Laurent, M., 1997. Neotectonic and seismic
716   activity in the Armorican and Cornubian Massifs: Regional stress field with glacio-
717   isostatic influence? J. Geodyn. 24, 219–239.

718 Walker, S.J., Weiss, R.F., Salameh, P.K., 2000. Reconstructed histories of the annual mean
719   atmospheric mole fractions for the halocarbons CFC-11 CFC-12, CFC-113, and carbon
720   tetrachloride. J. Geophys. Res. 105, 14285.

721 Warner, M.J., Weiss, R.F., 1985. Solubilities of chlorofluorocarbons 11 and 12 in water and
722   seawater. Deep Sea Res. Part A. Oceanogr. Res. Pap. 32, 1485–1497.

723 Weiss, R.F., Price, B.A., 1980. Nitrous oxide solubility in water and seawater. Mar. Chem. 8,
724   347–359.

725 Wyns, R., Baltassat, J., Lachassagne, P., Legchenko, A., Vairon, J., 2004. Application of
726   proton magnetic resonance soundings to groundwater reserve mapping in weathered
727   basement rocks (Brittany, France). Bull. la Société Géologique Fr. 175, 21–34.

728

1 *Figure 1: a) Location map and regional geological map. Star symbol indicates the St Brice Field site,*

2 *48°25'N 1°22'W, alt. 90m a.s.l. (modified from Chantraine,* (Chantraine et al., 2001)*). b) Local*

3 *geological map with main lineaments identified (modified Dadet,* (Dadet et al., 1984) *& IGN©).*

4

5 *Figure 2: Geological conceptual model of the St Brice field site. a) Conceptual geological structure in a*

6 *3D diagram representation, b) local geological map and boreholes location and c) cross-section of the*

7 *structure perpendicular to the main identified lineament.*

8

9 *Figure 3 : Typical hydraulic head variations measured in the different boreholes at Saint-Brice and*

10 *precipitations measured during the same period. Rainfall was measured at the nearest*

11 *meteorological station located 30 kilometers from Saint-Brice.*

12

13 *Figure 4: Flowrate profiles in FC4 borehole under (a) ambient conditions (before pumping), measured*

14 *with a Heat-Pulse-Flowmeter, and (b) pumping conditions, measured with an Impeller Flowmeter*

15 *Geovista©. The blue straight line represents the modeled flow using Paillet solutions* (Paillet, 1998)*.*

16

17 *Figure 5 : Drawdown in the pumping well (F3, blue triangle dots), in observation wells intersecting the*

18 *fault zone aquifer (FC4, MFT80 and MFT20, gray points) and observation wells located in the shallow*

19 *aquifer (T1, T2, T3, T5, T6 and T7, black lines)*

20

21 *Figure 6 : Diagnostic plot in Log scales showing drawdown (blue straight line) normalized by flow rate*

22 *(s/Q), and its derivative (blue point symbol) measured during the long term pumping test in F3.*

23

24   *Figure 7: Flow and temperature profiles under ambient (grey lines) and pumping conditions (after 9*

25   *and 63 days of pumping) in observation well (MFT80).*

26

27   *Figure 8 : Drawdown (s) evolution with time and its derivative (s') during pumping. Observations*

28   *come from MFT80 observation well. Moench and Boulton (modified Hunt) analytical models were*

29   *used to fit both drawdown and derivative curves. In a) only the first ten days were fitted while in b)*

30   *Moench's model was fitted to pumping results obtained at later times.*

31

32   *Figure 9 : Apparent age of water sampled at the outflow and deduced from CFC analysis.*

33

34   *Figure 10 : Tracer test data between the shallow aquifer (MFT80, gray point symbol) and the deep*

35   *fracture (FC4, gray triangle symbol), modeled with the Welty and Gelhar solution (gray straight lines).*

36   *Parameters used in the model are presented in the table* (Welty and Gelhar, 1994)*.*

37

38   *Figure 11 : Conceptual model of groundwater flow at the St-Brice site under a) ambient conditions*

39   *and b) pumping conditions*

40

41   Table 1: Borehole descriptions

42

43   Table 2: Transmissivity results obtained by modeling borehole flow profiles using Paillet solutions
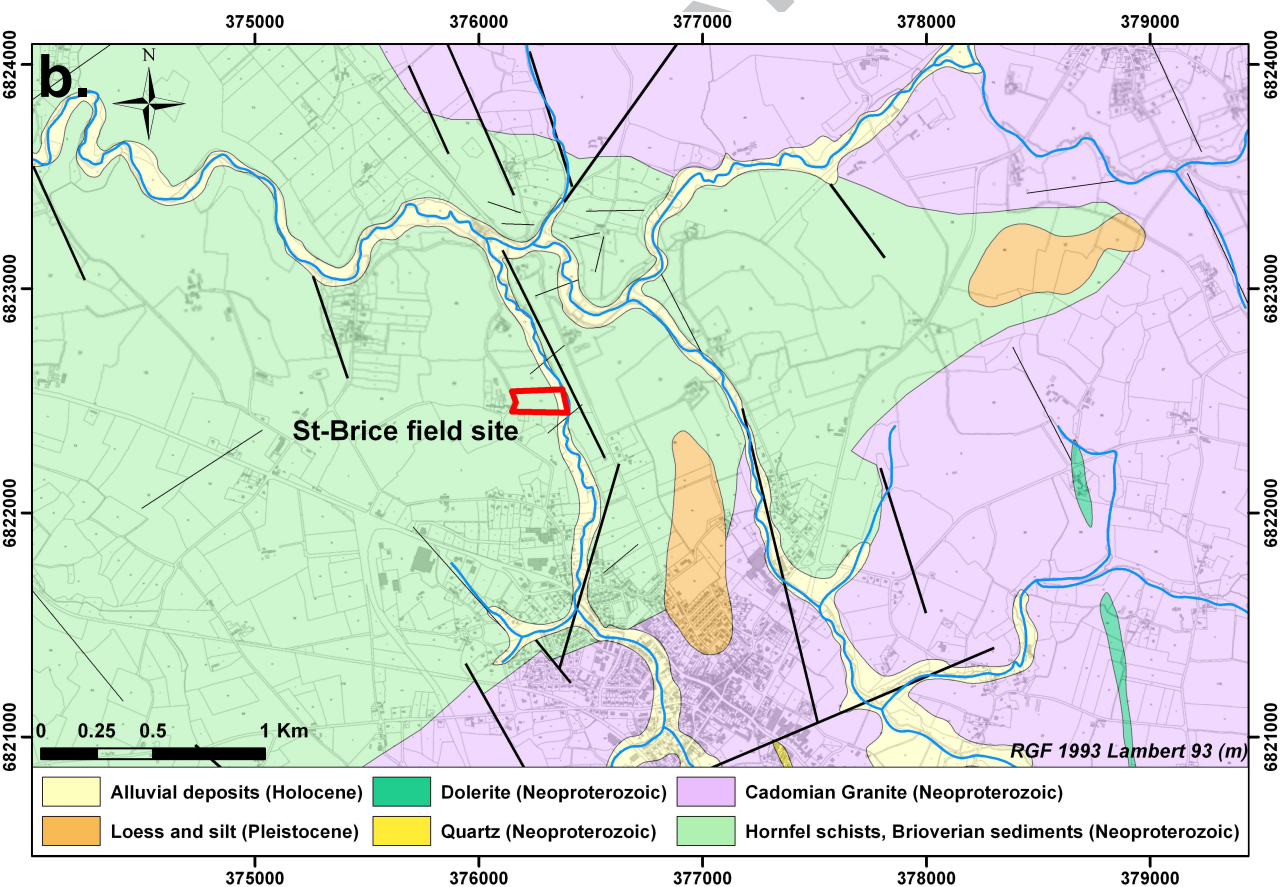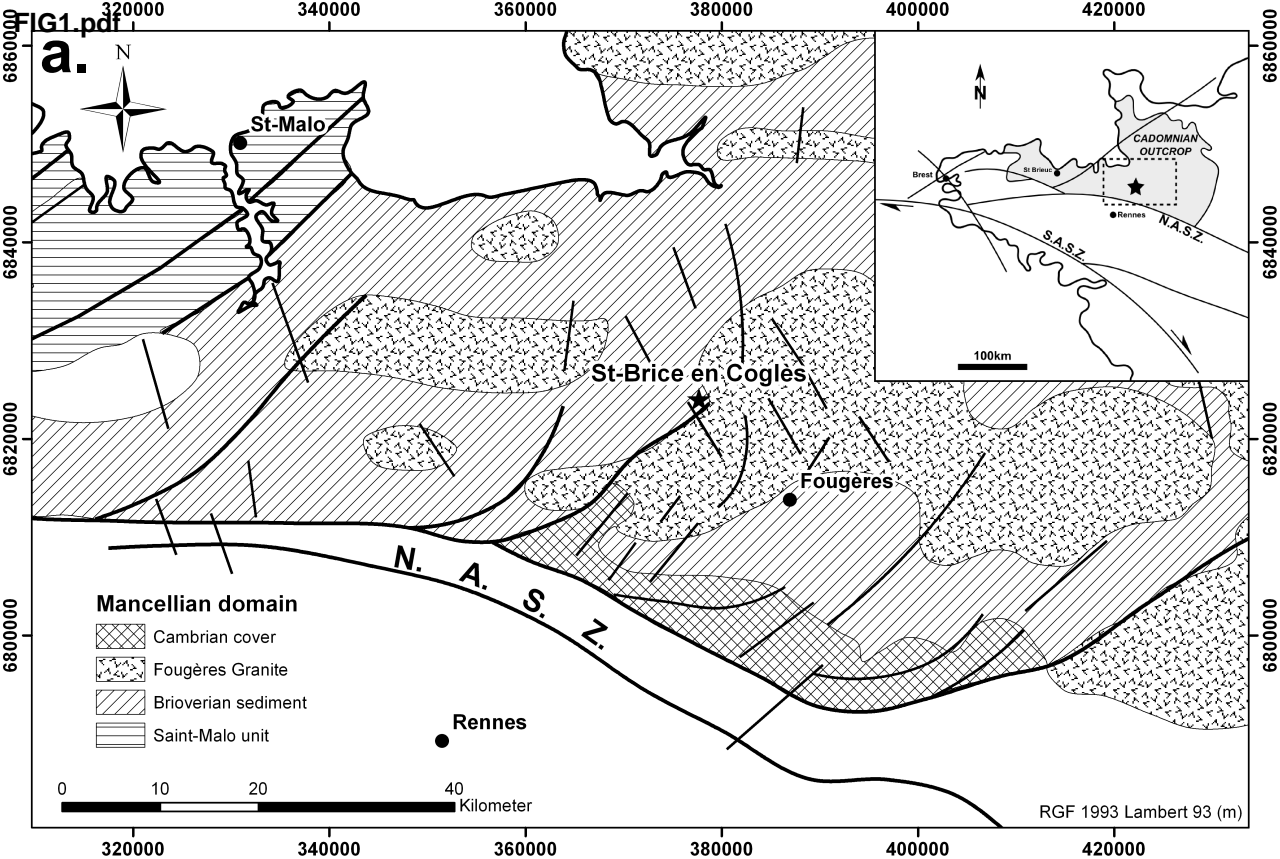
44   (Paillet, 1998).

45

46   Table 3: CFC and SF6 concentrations converted into atmospheric concentration (PPTV, (Bu and Mark

47   J Warner, 1995; M.J. Warner and Weiss, 1985)).

48

49   Table 4: Pumping test results for pumping well F3 and observation wells MFT80, FC4 and MFT20.

50   RMSE is calculated over the analyzed part of the pumping test.

51

FIG1.pdf

a.

St-Malo

St-Brice en Coglès

Fougères

N. A. S. Z.

Mancellian domain

- Cambrian cover
- Fougères Granite
- Brioverian sediment
- Saint-Malo unit

Rennes

0	10	20	40

Kilometer

RGF 1993 Lambert 93 (m)

Inset: CADOMNIAN OUTCROP, St-Malo, Brest, St Brieuc, Rennes, S.A.S.Z., N.A.S.Z., 100km

b.

St-Brice field site

RGF 1993 Lambert 93 (m)

Alluvial deposits (Holocene)

Loess and silt (Pleistocene)

Dolerite (Neoproterozoic)

Quartz (Neoproterozoic)

Cadomian Granite (Neoproterozoic)

Hornfel schists, Brioverian sediments (Neoproterozoic)

0	0.25	0.5	1 Km

Figure

Figure

FIG4.tif

FIG5.tif

Observation piezometers in weathered aquifer (<10m)

MFT20

MFT80

FC4

Observation wells in fractured zone.

Pumping well (F3)

Drawdown (m)

t-t0 (Days)

Figure

FIG8.pdf

FIG9.tif

Figure

	MFT80	FC4
Geometric Length (m)	53	135
Flow velocity (m/hr)	3.3	0.6
Porosity (%)	1.7	1.02
Dispersivity (m)	10	23
Peclet number	5.3	5.8

Legend: △ Data FC4; ○ Data MFT80; —— Model Becker and Charbeneau (2000)

Axes: C/C0 [-] versus t-t0 [h]

Figure

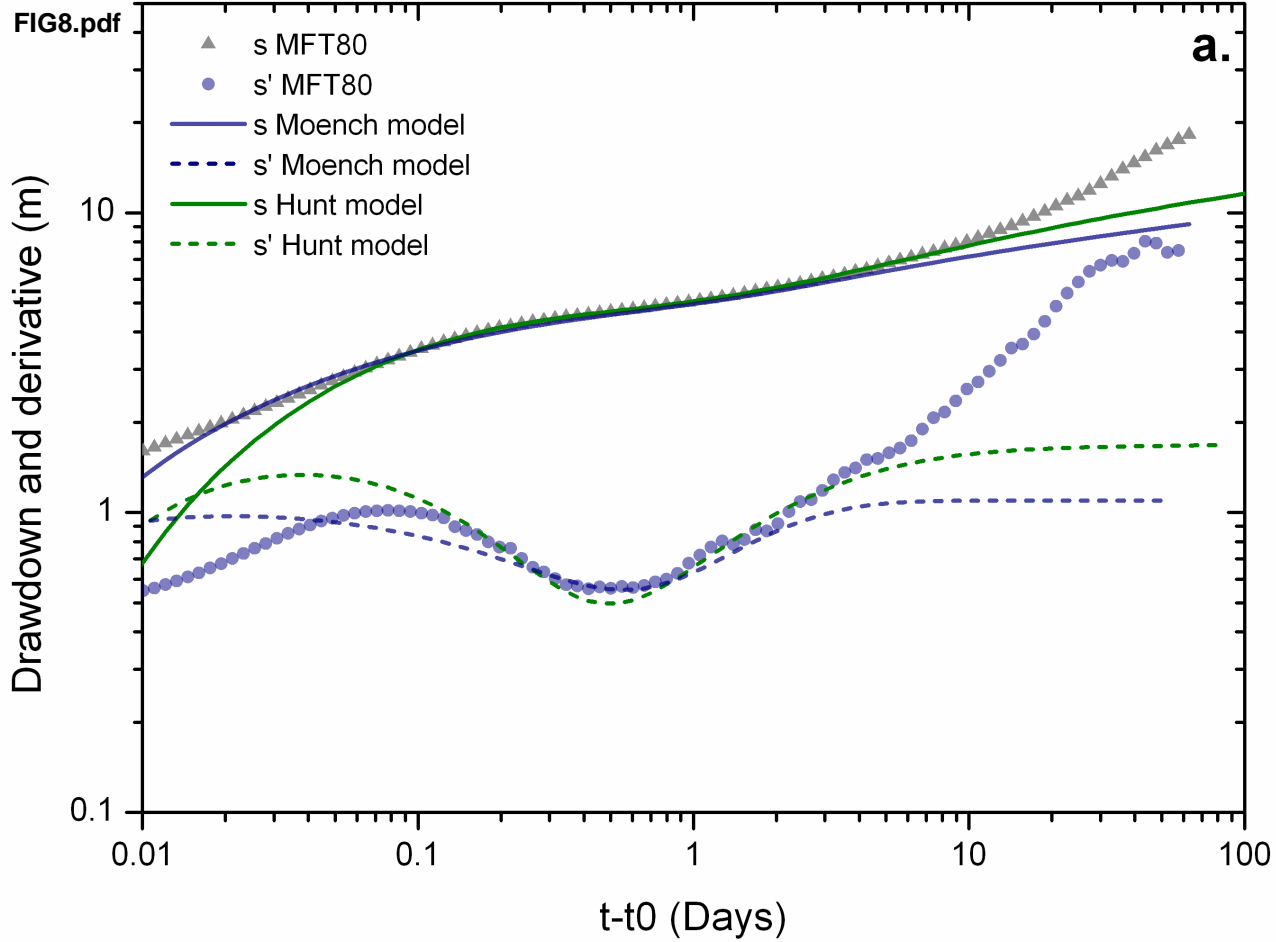| Well	X (LAMB93)	Y (LAMB93)	Z (a.s.l.)	Depth (m)	Geology	Slotted zone (m)	Main fracture depth (m)
F3	376280	6822515	93.53	216	Brioverian bed rock	30 to 216	110; 135 ;160; 169; 180; 192
FC4	376252	6822521	95.1	250	Brioverian bed rock	40 to 250	160; 204; 235
MFT20	376286	6822500	93.68	20	Brioverian bed rock	10 to 20	-
MFT80	376305	6822511	91.14	80	Brioverian bed rock	30 to 80	52; 69
T1	376350	6822537	88.22	6	Alluvial deposits (wetland)	1 to 6	-
T2	376353	6822504	88.27	8	Alluvial deposits (wetland)	2 to 6	-
T3	376329	6822490	89.57	6	Alterites	3 to 6	-
T4	376255	6822496	95.55	8	Alterites	4 to 8	-
T5	376294	6822485	93.54	7	Alterites	4 to 7	-
T6	376314	6822530	89.63	7	Alterites	2 to 6.5	-
T7	376273	6822531	93.02	9	Alterites	5 to 9	-
T8	376389	6822521	88.06	3	Alluvial deposits (wetland)	0.5 to 3	-

Well	Depth of fault zone (m)	Ambient Flowrate (L/mn)	Total transmissivity (m²/s)	Fractured zone transmissivity (m²/s)	Part of total productivity
FC4	235	3.5	1.3×10^{-3}	9.8×10^{-4}	75%
F3	90-116	3.5	1.8×10^{-3}	8.8×10^{-4}	50%
MFT80	48-53	2	7.9×10^{-4}	5.9×10^{-4}	75%

TABLE3.xls

Well	SF6 (pptv)	CFC-12 (pptv)	CFC-11 (pptv)	CFC-113 (pptv)
F3	0	50.13	6.03	14.47
FC4	0	19.85	5.83	31.04
MFT20	0.87	48.29	6.64	21.48
MFT80	0.5	52.93	5.11	24.22
T's (mean)	2.79	458.79	271.52	56.66

TABLE4.xls

Wells	Analytical models	Fault aquifer		Blocks parameters		Superficial aquifer			Error
		T (m²/s)	S (dless)	Kb (m/s)	Sb (1/m)	T0 (m²/s)	Sy (dless)	Kv (m/s)	RMSE [m]
F3	Moench early time	7.00E-04	-	2.47E-08	2.62E-04	-	-	-	0.98
	Hunt early time	4.79E-04	-	-	-	8.13E-05	-	-	0.55
	Moench global	**1.05E-04**	**7.00E-03**	**-**	**-**	**-**	**-**	**-**	***0.95***
MFT80	Moench early time	7.38E-04	7.00E-04	1.34E-09	1.15E-05	-	-	-	0.59
	Hunt early time	4.84E-04	1.80E-03	-	-	8.10E-05	0.02	1.09E-07	0.37
	Moench global	**9.03E-05**	**1.75E-03**	**1.28E-08**	**1.18E-03**	**-**	**-**	**-**	***0.56***
FC4	Moench early time	6.25E-04	8.40E-04	8.47E-10	9.84E-06	-	-	-	0.93
	Hunt early time	3.87E-04	1.61E-03	-	-	6.94E-05	0.02	8.00E-08	0.21
	Moench global	**1.13E-04**	**1.61E-03**	**8.15E-09**	**6.53E-04**	**-**	**-**	**-**	***0.57***
MFT20	Moench early time	6.02E-04	1.05E-02	3.35E-08	2.62E-04	-	-	-	0.69
	Hunt early time	7.27E-04	1.17E-02	-	-	5.79E-05	0.05	8.04E-07	0.19
	Moench global	**9.78E-05**	**7.00E-03**	**6.33E-08**	**3.07E-03**	**-**	**-**	**-**	***0.57***

Wells	Analytical models	Fault aquifer		Blocks parameters		Superficial aquifer			Error
		T (m²/s)	S (dless)	Kb (m/s)	Sb (1/m)	T0 (m²/s)	Sy (dless)	Kv (m/s)	RMSE [m]
	Moench early time	7.00E-04	-	2.47E-08	2.62E-04	-	-	-	0.98
	Hunt early time	4.79E-04	-	-	-	8.13E-05	-	-	0.55
	Moench global	1.05E-04	7.00E-03	-	-	-	-	-	0.95

1   We propose hydrogeological conceptual model of fault aquifer in crystalline basement.

2   We characterize interactions between a fault aquifer and surrounding compartments.

3   Sub-vertical fault resource is strongly dependent on superficial aquifer storage.

4   We estimate groundwater resource availability.

FRACTURED ZONE OUTCROPPING

RIVER

WETLAND

FC4

F3

MFT20

T5

MF180

T3

T2

T8

70%

30%